Dalton Transactions

Accepted Manuscript

ROYAL SOCIETY OF CHEMISTRY

www.rsc.org/dalton

Preparation and Crystal Structure of $K_2Ce(PO_4)_2$: A New Complex Phosphate of Ce(IV) Having Structure With One-Dimensional Channels

Samatha Bevara,[1,2] S. Nagabhusan Achary,[1,2] Sadiqua J. Patwe,[1] Anil K. Sinha,[2,3] and Avesh Kumar Tyagi[1,2]

[1]*Chemistry Division, Bhabha Atomic Research Centre, Mumbai 400085, India*

[3]*Indus Synchrotrons Utilization Division, Raja Ramanna Centre for Advanced Technology, Indore 452013, India*

[2]Also affiliated to:

Homi Bhabha National Institute,

Anushakti Nagar, Mumbai 400094

India

* Corresponding author

Dr. S. N. Achary
Chemistry Division, Bhabha Atomic Research Centre
Mumbai, 400 085, INDIA
Phone: 0092-22-25592328; Fax: 0091-22-25505151
Email sachary@barc.gov.in; acharysn@rediffmail.com (Dr. S. N Achary)

Abstract

In this manuscript we report crystal structure of a new complex binary phosphate $K_2Ce^{4+}(PO_4)_2$ in K_2O-P_2O_5-CeO_2 system prepared by solid state reaction at moderate temperature conditions. The prepared material was characterized by powder x-ray diffraction using lab source and synchrotron radiation as well as thermal analyses, Raman scattering, FTIR, and x-ray photoelectron spectroscopic studies. The crystal structure of the compound has been determined from powder XRD data by *ab initio* structure solution in direct space followed by Rietveld refinements. $K_2Ce(PO_4)_2$ crystallizes in a monoclinic ($P2_1/n$) lattice with unit cell parameters: a = 9.1060(4), b = 10.8160(5), c = 7.6263(4) Å, β = 111.155(2)°, V = 700.50(6) $Å^3$. The unit cell contains two distinguishable PO_4 tetrahedra and one CeO_8 distorted square anti-prism. Raman spectroscopy confirmed the presence of isolated PO_4^{3-} groups in the structure. These PO_4 tetrahedra are connected to one CeO_8 polyhedra by sharing one edge and three other CeO_8 polyhedra by sharing corners to form the three dimensional structure and empty channels parallel to *a*-axis. The channels are occupied by two crystallographically distinguishable K^+ ions which maintain the charge neutrality. Contrast to the earlier reported composition $K_4Ce_2P_4O_{15}$, this study revealed the composition in actual is $K_4Ce_2P_4O_{16}$ with Ce in 4+ oxidation state and is also supported by x-ray photoelectron spectroscopic and x-ray absorption near edge structure studies. Differential scanning calorimetric studies revealed a structural transition around 525°C which reverts on cooling with a large thermal hysteresis. At higher temperature it undergoes a loss of oxygen atom and subsequently loss of phosphorus as P_2O_5. These thermal effects are also supported by *in situ* high temperature XRD studies. Finally the crystal chemistry of complex phosphates with tetravalent cations is also discussed.

I. INTRODUCTION

Crystalline inorganic phosphates have been considered as an important class of materials due to their diversified crystal chemistry depending on composition, preparation condition as well as external parameters like temperature and pressure. In addition, they possess interesting physical properties amenable for varieties of technological applications. Several of the complex phosphate lattices, like apatite, zircon, monazite, cheralite etc. as well as nasicon type and zirconium phosphate have been considered as potential host matrices for immobilization of radioactive elements separated from the high level nuclear waste (HLW) due to their rock analogous properties viz. high thermal and chemical stability, high radiation resistance and insignificant leachability by water.[1-8] Rich crystal chemistry of phosphates with the variation of nature and ionic radius of cations have been explored in several reports.[6-8] In particular such phosphates with tetravalent ions form densely packed structure and they are amenable for immobilization of various actinides, like uranium, neptunium and plutonium. Besides, the complex phosphates with layer and tunnel structures having appropriate exchangeable ions have been considered as promising materials for selective separation of radioactive ions from high level nuclear waste or heavy metal ion pollutants from environment.[9-11] A large numbers of studies have demonstrated efficient exchange or sorption properties for separation of various ions from aqueous solution in a wider range of pH.[6] In particular, orthophosphates of Zr^{4+}, Ti^{4+} and Sn^{4+} as well as rare-earth ions or alkali and alkaline-earth metal ions are being considered for such applications due to their ion-exchangeability with various radioactive elements.[9-12]

Also, studies on such complex phosphates with suitable luminescent ions bear significant interest in the fundamental understanding of optical properties as well as technological relevant optical materials, like efficient x-ray scintillation, luminescent materials for plasma display panel as well as for lightening and stimulated emission applications. [13-19] In these regards, phosphates have been considered to be promising materials owing to their efficient absorption in vacuum ultraviolet region of common rare gas discharge excitation sources like Xe/Ne or He plasma and wide optical band gaps. [17,19,20] A number of such phosphates have been explored both theoretically and experimentally, where absorption around 7 to 9 eV due to O2pπ to P3p and O2pσ-P3s transitions have been concluded. [17,19-21] It has also been pointed out that the energy

absorbed in vacuum ultraviolet region is efficiently transferred to suitable luminescent ions, like Ce^{3+}, Eu^{3+}, Pr^{3+}, Tb^{3+} etc. [15-22] Several single phase complex phosphates in $MO–RE_2O_3–P_2O_5$ and $A_2O–RE_2O_3–P_2O_5$ (where M, A and RE are alkaline-earth, alkali and rare-earth ions respectively) systems have been explored and their potential for white or multicolour light emission have been demonstrated in these studies. [15-22] Compared to complex phosphates of alkaline earth metal ions, the complex phosphates with alkali metal ions are relatively less explored. [23,24] Hence delineation of new material in such system is an important aspect of crystal chemistry of phosphates.

Among the complex phosphates of tetravalent cations, studies with Ce^{4+} are limited due to its structural complexity as well as instability of the tetravalent Ce^{4+} ions in phosphate matrix.[25-29] Though the structural chemistry of Ce^{4+} has been extensively studied in oxide matrix, studies are limited with acidic groups like phosphates, vanadates etc. as they easily transform from Ce^{4+} to Ce^{3+} state.[25,30] However analogous phosphates with U^{4+}, Th^{4+}, Pu^{4+} are widely observed in phosphate matrix, which can be attributed to their higher stability in wider chemical environment.[3,9,10,31-38] Higher stability and low leachability of these phosphates make them suitable and stable matrix for incorporation of U^{4+}, Th^{4+}, Pu^{4+}.[1,2,6-8,36-38] Formation of phosphates with Ce^{4+} in CeP_2O_7 lattice is known and has been explored for negative thermal expansion, mixed ionic and electronic conduction as well as catalytic properties.[35,39,40] For latter two applications, the presence of mixed oxidation states and easier variation of oxidation states are the key features possessed by them. However at higher temperature, the Ce^{4+} reduces to Ce^{3+} and thus the structure of CeP_2O_7 collapsed by formation of Ce^{3+}. Despite the phosphates and vanadates of Ce^{4+} can be good host lattices for various luminescent ions, in particular trivalent lanthanide ions, they have not been explored significantly due to their limited stabilities.

Though the phosphates of Ce^{4+} are likely to have several practical applications, their existences are limited and thus they remain under explored. Some of the well characterized tetravalent phosphates of cerium reported in literatures are: $Na_{10}Ce_2P_6O_{24}$,[25] $(NH_4)_2Ce(PO_4)_2H_2O$,[27] $Ce(PO_4)(HPO_4)_{0.5}(H_2O)_{0.5}$[26,28] $Ce(PO_4)1.5(H_2O)(H_3O)_{0.5}(H_2O)_{0.5}$,[29] etc. Most often, low temperature processing conditions stabilize the Ce^{4+} in phosphate matrix while at higher temperature or in acidic conditions only Ce^{3+} is stabilized. Stabilization Ce^{4+} with

mixed PO_4^{3-} and HPO_3^{2-} ions has also been reported in literatures.[26,28,29] Hydrothermal methods are mostly used for the preparation of such complex phosphate moieties. [26-29] Coexistence of Ce^{3+} and Ce^{4+} in monazite type structures has been observed in compositions having P/Ce ratio in the range of 1.06 to 1.16. [41] Systematic studies of Popa et al. [42] revealed that most of the tetravalent cation except Ce^{4+} form double phosphate with Ba^{2+}. Authors also suggested that most of the claimed Ce^{4+} double phosphates indeed have Ce^{3+} ions only. Xu et al. have prepared hydrated ceric phosphate as $K_2Ce(PO_4)_2H_2O$ by hydrothermal method and characterized it by powder XRD and Raman spectroscopy. [43] Though the presence of isolated PO_4^{3-} group in it has been confirmed by vibrational spectroscopic investigations, detailed structure of this compound is not reported till date. For the structure of $K_2Ce(PO_4)_2H_2O$, an orthorhombic lattice with unit cell parameters as: a = 12.79(3), b = 15.01(5) and c = 16.94(3) Å have been assigned by them. [43] A closely related composition with K:Ce in 2:1 ratio, as $K_4Ce_2P_4O_{15}$ has been extensively investigated by Szczygiel.[44-38] and +3 oxidation state for cerium has been suggested. However, authors clearly mentioned that this compound can be easily obtained by solid state reaction of CeO_2 and with binary phosphates, like KPO_3.[45,46] Authors have also mentioned that the compound forms with $(NH_4)Ce^{3+}(NO_3)_4$ only at lower temperature and gets dissociated at higher temperature. [45] The crystalline product obtained by solid state reaction of CeO_2 and KPO_3 or KH_2PO_4 has been characterized by powder XRD and a triclinic lattice with unit cell parameters as: a = 9.319(7), b= 12.129(3), c= 9.252(1) Å, α = 106.875, β = 100.086, γ = 107.202°, has been assigned for it. Being ionic natures of such alkali metal ion containing compounds, they may be promising material for selective exchange of cations. Salvado et al. have prepared a complex phosphate of Ce^{4+} as $(NH_4)_2Ce(PO_4)_2H_2O$ and elucidated its crystal structure in detail. [27] This study revealed an orthorhombic zircon related structure for it, but the assigned unit parameters do not show any similarity with the reported orthorhombic unit cell parameters of $K_2Ce(PO_4)_2H_2O$. [43] Ogorodnyk et al. [49] have obtained a new complex phosphate with mixed Ce^{4+} and Zr^{4+}, as $K_4CeZr(PO_4)_4$, from high temperature molten flux synthesis and the structure has been elucidated from single crystal studies. A tetragonal ($I4_1$/amd) lattice with unit cell parameters closely similar to those of orthorhombic $(NH_4)_2Ce(PO_4)_2H_2O$ reported by Salvado et al. [27] has been assigned for $K_4CeZr(PO_4)_4$. The structural details of these studies indicate that both the compositions have zircon related structure and they can be considered as a super structure of zircon lattice. In both of these cases, the Ce^{4+} forms an eight coordinated polyhedra

and linked to PO_4 by sharing edges and corners in a closely similar manner as in zircon and monazite.[1,6-8]

Consideration of the structural analogies of reported complex phosphates with monovalent and tetravalent cations in 2:1 as well as reproducible preparation of $K_4Ce_2P_4O_{15}$ from CeO_2 suggest a possible existence of anhydrous complex phosphate with Ce^{4+}. In the aim to prepare and to understand the existence of complex phosphate with Ce^{4+} with alkali metal ions a composition with 2:1 ratio was prepared by a procedure similar to that adopted by Szczygiel [44-48] and characterized in detail. The present studied compound shows almost similar XRD pattern as that reported by the Szczygiel, [45] but all the observed peaks could be indexed on a monoclinic lattice contrast to the earlier assigned triclinic lattice. Further the structure of this composition has been obtained from the powder XRD data and the formation of $K_4Ce_2P_4O_{16}$, i.e. $2K_2Ce(PO_4)_2$ has been established instead of $K_4Ce_2P_4O_{15}$ as reported in literature. The presence of isolated PO_4^{3-} group and no $P_2O_7^{4-}$ is also confirmed in its structure. Thermoanalytical characterization revealed the presence of a structural transition in this compound. Details of the structure as well as high temperature behavior are explained in subsequent sections.

II. EXPERIMENTAL

The title sample was prepared by solid state reactions of stoichiometric amounts of KPO_3 or KH_2PO_4 and CeO_2. In the reaction with KH_2PO_4, 50 mmol of KH_2PO_4 and 25 mmol of CeO_2 were mixed together and then melted on a hot plate for about 3h. The obtained product was reground and heated at 500°C for 12h. The product was homogenized and pelletized. The pellet was heated at 750°C for 24h and cooled to room temperature. For other reaction, KPO_3 was prepared by decomposing KH_2PO_4, and 50 mmol of prepared KPO_3 was mixed with 25 mmol CeO_2. Thoroughly mixed powder was pressed into pellets and heated at 500°C for 12h. The product obtained after this reaction was rehomogenized, pelletized and then heated at 750°C for 24h. Since, the preparation procedure involved multi step heating protocols, attempts were made to minimize the loss during grinding and pelletization steps. The final yield is about 95 % of the expected mass.

The powder XRD pattern of the final product was recorded on a rotating anode based powder x-ray diffractometer using Cu Kα radiation. Formation of a new phase is confirmed by comparing the observed XRD pattern with those reported for various reactants as well as various known binary phosphates. For structural studies, powder diffraction data was collected in the two theta range of 10-100°, with a step width and time 0.02 and 3 sec, respectively. Powder XRD data of the sample was also recorded by using synchrotron radiation on the ADXRD beamline (on bending magnet port no BL-12) of Indus-2 (2.5 GeV, 100 mA) Synchrotron Radiation (SR) source (wavelength 0.8584 Å) at Raja Ramanna Centre for Advanced Technology (RRCAT), Indore, India. An image plate (mar 345) was used for recording the scattered x-ray beam and the diffraction image was integrated by using FIT2D program. [50] The obtained 2D XRD patterns were analyzed by using Fullprof-2K and *ab initio* structure solutions by simulated annealing methods. [51,52]

Thermogravimetric analyses were carried out on a thermobalance (SETARAM Instrumentation, France) and differential scanning calorimetric (DSC) measurement were carried out by using DSC (Mettler Toledo, Germany). Infrared (IR) absorption spectrum of the sample was recorded from 400 to 4000 cm^{-1} on a FT-IR spectrometer (JASCO Corp, USA) in transmission mode. Thin transparent pellets of mixture of sample and KBr were used for FTIR studies. For Raman scattering studies fine powder was smeared to uniform thick layer on a glass slide. Raman measurements were performed in backscattering geometry with a Horiba Jobin Yvon LabRAM HR UV microspectrometer (Japan) equipped with an edge filter and thermoelectric-cooled multichannel CCD detector. The 632.8 nm line of the HeNe laser with a power of 10 mW was used as excitation source for Raman scattering measurements. X-ray photoelectron spectrum (XPS) of the sample was recorded on an ESCA analytical instrument (Specs Surface Nano Analysis, Germany), by using a cold pressed pellet adhered to a carbon tape and Al Kα (1486.6 eV) x-ray as excitation source. The observed C 1s photoelectron peak was used as calibrant for correcting the binding energies. X-ray absorption near edge structure (XANES) spectra of CeO_2 and $K_2Ce(PO_4)_2$ were recorded in fluorescence mode at the same ADXRD beamline (BL-12) of Indus-2 synchrotron source, RRCAT, Indore, India. Powdered sample was placed between two kapton films. The thickness of the sample was about 0.2 mm. The incident photon flux was measured by an ionization chamber while the fluorescent photon

flux was measured by using a Peltier cooled energy dispersive detector (Vortex-Ex). Typical energy resolution (E/ΔE) of the beamline is 8000.

III. RESULTS AND DISCUSSION

The stoichiometric compositions prepared by direct solid state reactions of CeO_2 and KPO_3 as well as CeO_2 and KH_2PO_4 have bright yellow color. Identical XRD patterns for products of both reactions suggest the uniqueness of the final product. Since the product obtained by reaction of CeO_2 and K_2HPO_4 showed higher crystallinity, all further characterizations were carried out by using this sample. Typical powder XRD pattern of the final product of this reaction is depicted in **Figure 1**. In order to further confirm this phase, two more compositions with different K:P ratio were prepared under similar conditions and their XRD patterns are shown in ***Electronic Supplementary information*** **(ESI-1)**. In both of these additional compositions, Ce^{4+} of CeO_2 transformed to Ce^{3+} and thus they crystallize in structures analogous to the trivalent rare-earth ions. For further comparison, the powder XRD data reported for $K_2Ce(PO_4)_2H_2O$ [43] and $K_4Ce_2P_4O_{15}$ [45] are also included in **Figure-1**. The observed XRD pattern show similarity with that reported for $K_4Ce_2P_4O_{15}$, [35] suggesting that both the compositions may have similar crystal structures. Indexing of the observed peaks in the XRD pattern of present studied sample indicates a primitive monoclinic lattice with unit cell parameters: a = 9.106, b = 10.816, c = 7.616 Å, β = 111.16°. Comparing the unit cell volume and unit cell parameters, it could be inferred that the present observed phase is different from that reported earlier by Szczygiel. [45] It can be mentioned here that the intense reflections reported for $K_4Ce_2P_4O_{15}$ could be accounted in the present observed unit cell. Further characterization of the sample of present study by thermal techniques, explained below, indicated almost similar thermogravimetric curve as that reported for $K_4Ce_2P_4O_{15}$. [45]

Thermogravimetric curves of the prepared composition recorded while heating from room temperature to 900°C is shown in **Figure 2a**. It can be seen that the sample lose weight in two steps. The first step of weight loss is sharp, with an onset temperature of about 850°C. However, the second weight loss step overlaps with the first one at around 880°C. The initial weight loss amounting to 1.8 % can be accounted to a loss of one oxygen atoms and the

subsequent loss can be accounted to loss of P_2O_5 molecules. Szczygiel [45] has reported a similar two step weight loss for the $K_4Ce_2P_4O_{15}$ sample, but attributed for the loss of P_2O_5. The analysis of initial weight loss suggests the composition as $K_4Ce_2P_4O_{16}$ with all cerium in 4+ oxidation state. Around 880°C, the composition decomposes peritectically to $CePO_4$, $K_3Ce(PO_4)_2$ and P_2O_5. Xu et al. [43] have reported the decomposition behavior of $K_2Ce(PO_4)_2H_2O$ and suggested three weight losses, namely loss of water molecules forming an anhydrous phase around 175°C, decomposition accompanied by reduction of Ce^{4+} to Ce^{3+} around 850°C and subsequently, a peritectic decomposition to $K_3Ce(PO_4)_2$, $CePO_4$ and P_2O_5 around 880°C. DSC curves of the sample are shown in **Figure 2b.** An endothermic peak around 525°C attributable to a structural transition is observed in the heating step of DSC curve. A similar endothermic peak has been reported by Szcygiel for their $K_4Ce_2P_4O_{15}$ sample. [45] Xu et al. [43] have also reported a structural transition at around 500°C for the anhydrous product obtained from $K_2Ce(PO_4)_2H_2O$. Comparing results of Xu et al. [43] with the present observation, it can be concluded that the dehydration $K_2Ce(PO_4)_2H_2O$ leads to an anhydrous phases which is similar to that observed in present study as well as that of Szcygiel. [45] However, in both the earlier studies, structures of hydrated or anhydrous products were not investigated to confirm the composition. It can also be seen from the DSC curves, that the endothermic peak observed in heating cycle reverts back while cooling but with a large hysteresis in temperature. Thus the phase transition might be a reconstructive type with significant change in structure. The enthalpy of phase transition as obtained from the area of the DSC peak in heating cycle is 69.5 J/g. The observed enthalpy change is also close to that reported by Szcygiel. [45] Thus it is convincing that the composition studied by Szcygiel [45] is $K_4Ce_2P_4O_{16}$ and similar to the presently studied phase as well as the anhydrous phase of Xu et al. [43] Since the composition undergoes an irreversible decomposition process at higher temperature, no single crystal could be obtained for further study. Hence the structural studies from powder diffraction were carried out and they are explained below.

In order to confirm the phase transition observed in the sample, *in situ* high temperature XRD patterns were recorded. The XRD patterns recorded at some representative temperatures are shown in **Figure 3**. The XRD pattern recorded above 500°C show the formation of a new phase which is observed as single phase at 550 and 600°C. The original room temperature phase could be observed in the XRD pattern recorded after cooling. An increase in symmetry in the

phase transition is indicated by the well separated and resolved peaks in the XRD patterns recorded at high temperature. A simple comparison of the XRD pattern recorded at 600°C revealed its close similarity with those reported for tetragonal $K_2ZrCeP_2O_8$ [49] and orthorhombic $(NH_4)_2CeP_2O_8$ H_2O [27] phases. All the observed intense reflections could be accounted by an orthorhombic lattice with unit cell parameters: a = 6.829(1), b = 6.811(2), c = 17.487(2) Å, V = 813.4(3) $Å^3$. The structural transition is accompanied with about 14% increase in molar volume. The profile of the powder XRD data could be refined by Le bail profile refinement method using the space group *I*mma. Typical fitted XRD pattern of the high temperature phase is provided as ***supplementary data*** (ESI-2) to the manuscript.

Further to understand the decomposition reaction of $K_2Ce(PO_4)_2$, powder XRD pattern recorded after heating the sample at 900 °C for 5h was analyzed. The observed peaks in diffraction pattern could be accounted for $K_3Ce(PO_4)_3$ and $CePO_4$, which confirms decomposition reaction is: $6K_2Ce(PO_4)_2 = 4K_3Ce(PO_4)_2 + 2CePO_4 + P_2O_5 + 3(O)$. The transitional phase, formed by the loss of oxygen could not be isolated due to overlapping of oxygen loss and decomposition steps. The XRD pattern of the decomposed sample is given as ***Supplementary data*** (ESI-3) to the manuscript.

As mentioned earlier, the observed powder XRD pattern recorded by using CuKα radiation could be indexed on a primitive monoclinic cell. From systematic absences the space group $P2_1/n$ could be assigned. Further trials by *Le bail* refinement of powder XRD data with possible monoclinic symmetries confirmed that the space group $P2_1/n$ is most suitable symmetry. From the initial composition and observed unit cell volume, four molecules per unit cell were considered for analyses of the structure. Refinement of the powder XRD pattern in direct space formalism is initiated with the observed unit cell parameters and positions for two K, one Ce, two P and eight oxygen atoms. In the initial stage itself two phosphate groups could be easily located in the Monte-Carlo procedure. [52] Subsequently two PO_4 tetrahedral units were used in the optimization procedures. The converged refinements clearly indicated optimal positions for all K, Ce, P and O atoms. Using the optimized structural parameters, Rietveld refinements of the powder XRD data were carried out. Appreciably good agreement with observed and calculated XRD patterns could be obtained.

For further confirmation, the optimized structural model was used to refine the powder XRD pattern recorded by using synchrotron radiation. The background of the XRD pattern was refined by linear interpolation of selected points while the profile was modeled by *pseudo-Voigt* function. No preferred orientation correction but the absorption correction was applied by using angle dependent micro absorption correction method. [51] Refinement of unit cell parameters along with the profile parameters shows a good support for the obtained model structure. Finally all the position coordinates as well as isotropic thermal parameters were refined along with the profile parameters. In the SR XRD pattern, some weak reflections assignable to monoclinic $CePO_4$ were observed. The formation of $CePO_4$ indicates its higher stability compared to Ce^{4+} containing phosphates. Thus the structural parameters for monoclinic monazite type $CePO_4$ were included in the final refinement cycles. The final residuals of refinements are R_p = 5.45 %, R_{wp} = 6.44 %, and χ^2 = 2.97, which suggest good convergence of the structural parameters. The final Rietveld refinement plot is shown in **Figure 4** and refined structural parameters are given in **Table 1**. Typical inter-atomic distances and bond angles are given in **Table 2 and 3**, respectively. Typical tables for motifs of mutual adjunctions are given in ***Electronic Supplementary information* (ESI-4)** to this manuscript.

Analyses of the refined structural parameters of $K_2Ce(PO_4)_2$ indicates two distinct and nearly regular tetrahedral phosphate groups ($P(1)O_4$ and $P(2)O_4$) and one Ce in eight coordinated polyhedra with oxygen atoms. Typical P-O bond lengths in both PO_4 tetrahedra are in range of 1.55 to 1.56 Å as observed in regular orthophosphate groups. Typical Ce-O bond lengths are in the range of 2.20- to 2.54 Å (**Table-2**). Bond valence sum calculations for CeO_8 polyhedra indicates the total valence of Ce is 4.17 (R_o = 2.096, B = 0.37 are taken from *Ref .25*) which is in agreement for the Ce^{4+} ion in structure. This is further confirmed by the XPS results explained later. The $P(1)O_4$ and $P(2)O_4$ tetrahedra share one edge and two corners oxygen atoms with CeO_8 polyhedra and form a three dimensional lattice with tunnel like empty space along the <100> direction. The empty channels are occupied by two K^+ ions which balance the net charge in the structure. The observed K-O bond lengths are in the range of 2.52 to 3.05 Å (**Table-2**) and the separation between two K^+ ions is 3.35 to 3.44 Å (viz. K1-K1 = 3.436, K2-K2 = 3.353 and K1-K2 = 3.421 Å) which is similar to that reported by Ogorodnyk et al for $K_4CeZr(PO_4)_2$. [49] Within

the bond distance limit of 3.1 Å, both K(1) and K(2) can be considered as distorted and asymmetric eight coordinated polyhedra. The typical three dimensional structure of the $K_2Ce(PO_4)_2$ is shown in **Figure 5**. Typical local surrounding around the CeO_8 showing linked PO_4 tetrahedra is shown in **Figure 6**.

The presence of Ce^{4+} as concluded from the valency calculations is further confirmed from the XPS spectrum of the sample. The observed XPS spectra of the sample are shown in **Figure 7**. The characteristic 3d photoelectron spectra of the sample (marked in **Figure 7**) is closely similar to that reported for Ce^{4+} in CeO_2.[53,54] The presence of $3d_{5/2}$ satellite peak (u′′′) around 917 eV clearly indicate 4+ oxidation states of cerium in the sample. It needs to mention here that the composition $K_4Ce_2P_4O_{15}$ studied by Szczygiel et al. [44] does not have the characteristic u′′′ which suggests the composition has majority of Ce^{3+}. This may be due to the partial decomposition or any other unknown reasons. Kopa et al. [42] have compared the 3d photoelectron spectra of Ce^{3+} and Ce^{4+} and suggested a significant difference in line shapes of the peaks and noticeable differences in the intensity of the u ($3d_{3/2}$) and v′′′ ($3d_{5/2}$) peaks.[53] The observed line shape and intensities of u and v′′′ peaks of $K_2Ce(PO_4)_2$ further support for Ce^{4+}. Further support for oxidation state of cerium was obtained by comparing the L-II absorption edge of $K_2Ce(PO_4)_2$ and CeO_2. The normalized absorption for both XANES spectra for $K_2Ce(PO_4)_2$ and CeO_2 are shown in **Figure 8.** The L-II edge of CeO_2 is in agreement with that reported earlier in literature. [55] The characteristic absorption at L-II edge of Ce are closely similar in both the studied materials and thus supports for Ce^{4+} in $K_2Ce(PO_4)_2$. Thus it could be unequivocally concluded that the present studied composition is formed with Ce^{4+}.

The CeO_8 and PO_4 coordination polyhedra in the studied $K_2Ce(PO_4)_2$ phase are closely related to those reported earlier for tetragonal $K_4CeZr(PO_4)_4$ [49] and $(NH_4)_2Ce(PO_4)_2H_2O$. [27] Since the structure of orthorhombic $K_2Ce(PO_4)_2$ H_2O phase reported by Xu et al. [33] is still unknown, more conclusion on the transformation from orthorhombic to the present observed monoclinic phase could not be obtained. The edge and corner shared polyhedra in the present structure are similar to that observed in typical zircon and monazite-type phosphates of trivalent cations. [5,6-8,33] However, connections of these polyhedra and the extension of the $Ce(PO_4)_6$ units in the three dimensions is unique in the present structure compared to those reported for

$K_4CeZr(PO_4)_4$ and $(NH_4)_2Ce(PO_4)_2H_2O$ in literature. [27,49] A closer inspection of the structural arrangement indicates that the connection the two edges shared PO_4 units are closer compared to those reported for $K_4CeZr(PO_4)_4$ and $(NH_4)_2Ce(PO_4)_2H_2O$ as well as that in zircon, It can be mentioned here that the typical connection of CeO_8 and PO_4 in the present studied structure is similar to that in recently reported structures of $Na_{10}M_2(PO_4)_6$, where M = U^{4+} and Ce^{4+}. [25] Recently, polyhedra with such type of linkages are observed in some complex arsenates with composition as $A_2Th(AsO_4)_2$, A = Alkali ion. [56] Further comparison of the present studied $K_2Ce(PO_4)_2$ and $K_4CeZr(PO_4)_4$ indicates distinct differences in the local coordination, due to intermixing of smaller Zr^{4+} and larger Ce^{4+} ions in the latter. The differences in the ionic radii of the Zr^{4+} and Ce^{4+} favor for the six coordinated ZrO_6 and eight coordination CeO_8 polyhedra. Thus the two types of PO_4 polyhedra observed in the latter structure show orientational disorder. However no long range periodicity of Zr^{4+} and Ce^{4+} has been observed in this study.[49] An analogy of the structure of mixed phosphates of tetravalent cations indicates, cations like Zr^{4+} and Hf^{4+} and others smaller cations preferentially form octahedral MO_6 polyhedra and they are connected by the PO_4 units forming the three dimensional structure, while the larger cations like Ce^{4+}, Th^{4+} etc. prefer eight coordinated MO_8 polyhedra as the building unit.

Structural studies on $Na_2Th(PO_4)_2$ by Galesic et al. [57] indicated two closely related monoclinic structures, one with space group *C*2/c and other with space group $P2_1/n$. In both the polymorphs of $Na_2Th(PO_4)_2$, Th^{4+} ions form eight coordinated polyhedra within the Th-O bond length limit of 2.7 Å and P^{5+} ions from nearly regular tetrahedra. The reported unit cell parameters of both the phases of $Na_2Th(PO_4)_2$ are closely similar. The unit cell parameters of the presently studied $K_2Ce(PO_4)_2$ can be related to those reported for $Na_2Th(PO_4)_2$ by unit cell relations as: *a' = a, b' = 2b, c' = c,* where the prime indicates the parameters of Galesic et al. [57] The preliminary inspection of powder XRD pattern calculated from the model generated from $Na_2Th(PO_4)_2$ structures with corresponding unit cell parameters for $K_2CeP_2O_8$ shows significant differences in the intensity distribution. Further refinements of powder XRD pattern with this model lead to no success. Thus it can be concluded that the observed phase of $K_2Ce(PO_4)_2$ has distinct structural features compared to $Na_2Th(PO_4)_2$ [57] or $K_2CeZr(PO_4)_2$ [27,49] reported earlier. Comparison of these three structure types indicates distinct structural arrangements of MO_8 (M = Th, Ce or Ce/Zr) and PO_4 polyhedra in them. In the reported structures of $K_2CeZr(PO_4)_2$ [49] or

$(NH_4)_2Ce(PO_4)_2$, [27] the PO_4 tetrahedra are connected to MO_8 distorted bisdisphenoid by sharing two *trans* edges of latter while in the present structure of $K_2Ce(PO_4)_2$, the PO_4 tetrahedra share two *cis* edges of CeO_8 polyhedra. This arrangement is similar to that observed for $A_2Th(AsO_4)_2$, where A = K and Rb. [55] Interestingly the structure reported for $Na_2Th(PO_4)_2$ shows both kinds of connections with two crystallographically distinct Th^{4+} ions. [57] Typical structures depicting the differences in the polyhedral arrangements in these three compounds are shown in **Figure 6**. It can be mentioned here that the PO_4 groups in $K_2CeZr(PO_4)_2$ has orientational disorder due to differences in the size of Ce^{4+} and Zr^{4+}, while no such disorder is observed in $Na_2Th(PO_4)_2$. But two different symmetries are formed in $Na_2Th(PO_4)_2$ compounds due to ordering and disordering of Th^{4+} sites. Similar comparison with the reported structures of $Na_2Zr(PO_4)_2$ or $K_2Zr(PO_4)_2$ indicates a clear differences in them. In these Zr^{4+} analogous compositions, Zr forms octahedral units and they are connected to PO_4 by sharing its corner oxygen atoms only. [58] Thus it is reasonable to say that the inter-cation (M^{4+} and P^{5+}) repulsion favor for such corner connected polyhedral structure with such smaller tetravalent cations. It can be expected that the structural differences between $K_2Ce(PO_4)_2$ and $Na_2Th(PO_4)_2$ [57] may arise from the difference in ionic radii of Ce^{4+} (0.97 Å in coordination number 8) and Th^{4+} (1.05 Å, in coordination number 8). However, smaller the size of CeO_8 compared to ThO_8 should destabilize the *cis* connected MO_8 and PO_4 structure of the $K_2Ce(PO_4)_2$. The preliminary analyses of the structure of $K_2Ce(PO_4)_2$ at high temperature indicates a *trans* connected MO_8 and PO_4 structure and has a significantly larger volume compared to the structure of room temperature phase. Besides, the observation of a similar structure in $K_2Th(AsO_4)_2$ [55] as in the room temperature structure of $K_2Ce(PO_4)_2$, suggests nature of charge balancing counter cations, like Na^+ (radius 1.02 Å) or K^+ (ionic radius 1.38 Å) as well as preparation conditions might be the structure directing factors in the crystal chemistry of the phosphates of tetravalent ions. Thus the formation of structure $A_2M^{4+}(PO_4)_2$ is not only sensitive to the nature tetravalent (M^{4+}) cation but also to the ionic radii of A^+ ions. Also, it appears that the diverse structures of such mixed phosphates of alkali and tetravalent cations are due to ionic radii and local structure around the tetravalent cation.

From the observed structural features it can be inferred that $K_2Ce(PO_4)_2$ can be a better host lattice for various luminescent ions, in particular trivalent lanthanide ions, due to its closely similar ionic radius and local coordination polyhedra as well as non luminescent nature of Ce^{4+}.

Also, due to the presence of two types of tetrahedral PO_4 group, absorption in this lattice is expected to be in a broader region of vacuum ultra violet spectrum. The distorted cubic nature of Ce^{4+} site can allow the forbidden transitions of the luminescent ions as observed in other lattices. [18,59] Absorption in a wider spectral range has been reported in the complex phosphates of U^{4+}. [25] Analogous studies on single phase phosphates with octahedrally coordinated tetravalent cations indicate efficient full colour emission.[18,23,60,61] Additionally, the sites for K ions in $K_2Ce(PO_4)_2$ can be substituted by suitable cations to maintain the charge neutrality and hence oxygen defects in the lattice.

More information on the structural features of $K_2Ce(PO_4)_2$ were obtained from the Raman and IR spectroscopic studies. The observed Raman spectrum of $K_2Ce(PO_4)_2$ at room temperature is shown in **Figure 9,** which is closely similar to that reported by Szczygieł et al. for $K_4Ce_2P_4O_{15}$. [48] From group theoretical analyses, $K_2Ce(PO_4)_2$, space group $P2_1/n$, Z =4, has 156 vibration modes with mechanical representation as $\Gamma = 39A_g + 39A_u + 39B_g + 39B_u$ (153 optical, $\Gamma_{optic} = 39A_g + 38A_u + 39B_g + 37B_u$ and 3 acoustic, $\Gamma_{acoustic} = A_u + 2B_u$). The mechanical representations for the optical modes suggest 78 ($39A_g + 39B_g$) Raman active and 75 ($38A_u + 37B_u$) IR active modes. In the present Raman spectrum, 39 Raman modes could be clearly identified while other modes could not be observed either due to weak intensity or degeneracy origin overlapping. The FTIR spectrum of the sample is shown in **Figure 10**. The observed Raman and IR modes are given in **Table 4**. The absence of absorptions near 1600 and 3600 cm^{-1} in the IR spectrum, attributable to the bending and stretching vibrations of water confirms anhydrous nature of the studied sample and hence is different from the sample studied by Xu et al. [35] In addition no absorptions band around 1235 cm^{-1} due to P-OH bending vibration is observed in the IR spectrum. This confirms the absence of any OH group in the present studied sample. The modes are assigned in the analogy of Raman and IR spectra of various phosphates and pyrophosphates. Earlier Szczygiel et al. have analyzed the Raman and IR spectra by considering the PO_4^{3-} and $P_2O_7^{2-}$ groups. [48] In general, the symmetric and asymmetric stretching Raman modes of P-O-P linkage are observed around 735-745 cm^{-1} and 950-970 cm^{-1},[35,39,62-64] which are absent in present Raman spectrum. Thus the presence of $P_2O_7^{2-}$ as suggested by Szczygiel et al. [48] could not be confirmed. All the observed Raman modes are in agreement with PO_4^{3-} as concluded from the structural analyses discussed earlier. This is substantiated by the absence of modes in between

735-745 cm^{-1}, commonly assigned for $P_2O_7^{2-}$ group. [62-64] The observed modes of Raman spectrum can be grouped into three regions, the high frequency modes, mainly due to the internal modes of PO_4 group and low frequency modes are due to translational motions of K^+ and Ce^{4+} ions. The Raman modes observed in range of 1022-1129 cm^{-1} and 943-1000 cm^{-1} can be assigned to asymmetric (ν3) and asymmetric (ν1) stretching of the PO_4^{3-} group. Similarly, the modes observed in the intermediate range 312-461 cm^{-1} and 541-629 cm^{-1} are the symmetric and asymmetric bending modes of PO_4^{3-} group. The lattice modes (wave number below 312 cm^{-1}) are mainly due to translational motion of the K^+ ions in the oxygen polyhedra. The typical assignments of the modes are summarized in the **Table 4.** The Raman spectrum recorded at higher temperature, 580°C, (shown in ***Supplementary information*** **(ESI-5)** is closely similar to that recorded at room temperature but the modes in all three regions are broadened. This suggests the local coordination in both room temperature and high temperature are closely similar, but structure at higher temperature is disordered or more likely a higher symmetric structure as suggested by high temperature XRD studies.

IV. CONCLUSION

From the systematic structural and vibration spectroscopic studies, the existence of a new mixed phosphate with Ce^{4+} ions in the K_2O-P_2O_5-CeO_2 system have been established. The compound exists at moderate temperature and decomposed peritectically above 850°C. This decomposition is attributed to a loss of oxygen due to reduction of Ce^{4+} to Ce^{3+}. The composition shows clear differences from the phase reported earlier in literature and bears a close relation with the other isocompositional phases of tetravalent actinide or lanthanides ions. Complete structure of the present investigated phase could be obtained from powder XRD data. A complex arrangement of PO_4^{3-} and CeO_8 form the frame of the structure. The one dimensional channels formed in this frame are filled with the K^+ ions for charge neutrality. It is also concluded the present observed structure is different from the earlier reported tetragonal and orthorhombic phases of $K_2Ce(PO_4)_2$ and monoclinic phases of $Na_2Th(PO_4)_2$. However, the present structure is closely similar to that reported of $K_2Th(AsO_4)_2$ and $Rb_2Th(AsO_4)_2$. The identified phase is a new complex phosphate with Ce^{4+} and structural architect indicates a possible host material for various luminescent ions as well as a potential material for ion exchanging applications.

ACKNOWLEDGMENTS

Authors thank Dr. V. K. Jain, Head Chemistry Division, BARC, for his interest and supports to this work. Also authors thank Dr. R. Mishra, Chemistry Division, BARC, for extending the thermal analysis facility for this study. Dr. K. Bhattacharya, Dr. A. K. Tiapathi and Dr. S. R. Bhardwaj of Chemistry Division, BARC are also thanked for providing the XPS data for this study.

†Electronic Supplementary Information (ESI) available: ESI-1. Typical XRD patterns of different compositions in K_2O-P_2O_5-$CeO_{2/1.5}$ system. ESI-2. Typical fitted XRD pattern of $K_2Ce(PO_4)_2$ recorded at 600°C. ESI-3. Typical XRD pattern of $K_2Ce(PO_4)_2$ recorded after heating a 900°C for 5h. ESI-4. Table of motifs of mutual adjunction of $K_2Ce(PO_4)_2$ and related compounds. ESI-5. Typical Raman spectra of $K_2Ce(PO_4)_2$ recorded at different temperatures. More details of structural parameters can be obtained from the Fachinformationszentrum Karlsruhe, Abt. PROKA, 76344 Eggenstein-Leopoldshafen, Germany (fax +49-7247-808-666; E-mail: crysdata@fiz-karlsruhe.de) by quoting the CSD number 429910.

References

1 L. A. Boatner and B. C. Sales, Monazite in: Radiation Waste Forms for the Future (W Lutze, and R. C. Ewing, eds) North-Holland, Amsterdam **(1988),** p. 495-564.

2 L. Bois, M. J. Guittet, F. Carrot, P. Trocellier, and M. Gautier-Soyer, *J. Nucl. Mater.,* 2001*,* **297**, 129.

3 N. Clavier, N. Dacheux, and R. Podor, *Inorg. Chem.,* 2006, **45**, 220.

4 N. Clavier, N. Dacheux, G. Wallez, and M. Quarton, *J. Nucl. Mater.,* 2006, **352**, 209.

5 S. N. Achary, D. Errandonea, A. Munoz, P. Rodríguez-Hernandez, A. Manjon, P. S. R. Krishna, S. J. Patwe, V. Grover, and A. K. Tyagi, *Dalton Trans.,* 2013, **42**, 14999.

6 D. Bregiroux, K. Popa, and G. Wallez, *J. Solid State Chem.,* 2015, **230**, 26.

7 D. Bregiroux, G. Wallez, and K. Popa, *Solid State Sci.,* 2015, **41**, 43.

8 D. Bregiroux, K. Popa, R. Jardin, P. E. Raison, G. Wallez, M. Quarton, M. Brunelli, C. Ferrero, and R. Caciuffo, *J. Solid State Chem.,* 2009, **182**, 1115.

9 A. Clearfield, *Chem. Rev.,* 1988, **88,** 125.

10 K. Popa, R. J. M. Konings, T. Wiss, and H. Leiste, *J. Radioanal. Nucl. Chem.,* 2007*,* **273**, 563.

11 I. A. Stenina, A. D. Aliev, I. V. Glukhov, F. M. Spiridonov, and A. B. Yaroslavtsev, *Solid State Ionics,* 2003, **162-163,** 191.

12 C. Trobajo, M. L. Rodríguez, M. Suárez, J. R. García, J. Rodríguez, J. B. Parra, M. A. Salvadó, P. Pertierra, and S. García-Granda, *J. Mater. Res.,* 1998, **13**, 754.

13 P. Arunkumar, C. Jayajothi, D. Jeyakumar, and N. Lakshminarasimhan, *RSC Adv.,* 2012, **2**, 1477.

14 E. M. Villa, C. J. Marr, F. J. Jouffret, E. V. Alekseev, W. Depmeier, and T. E. Albrecht-Schmitt, *Inorg. Chem.,* 2012, **51**, 6548.

15 P. Vergeer, T. J. H. Vlugt, M. H. F. Kox, M. I. den Hertog, J .P. J. M. vander Eerden, and A. Meijerink, *Phys. Rev. B* 2005, **71**, 014119.

16 J. L. Yuan, X. J. Wang, and J. T. Zhao, China Patent, *Appl. No. 200610024554.0.*

17 J. L. Yuan, X. J. Wang, D. B. Xiong, C. J. Duan, J. T. Zhao, Y. B. Fu, G. B. Zhang, and C. S. Shi, *J. Lumin.,* 2007, **126**, 130.

18 D. Wisniewski, A. J. Wojtowicz, W. Drozdowski, J. M. Farmer, and L. A. Boatner. *Cryst. Res. Technol.,* 2003, **38**, 275.

19 S. Chen, Y. Wang, J. Zhang, L. Zhao, Q. Wang, and L. Han, *J. Lumin.,* 2014, **150**, 46.

20 Y. Wang and D. Wang, *J. Solid State Chem.,* 2007, **180**, 3450.

21 G. Lakshminarayana, T. D. Dao, K. Chen, M. Sharma, T. Takeda, M. G. Brik, I. V. Kityk, S. Singh, and T. Nagao, *Opt. Mater.*, 2015, **39**, 110.

22 M. -R. Li, W. Liu, H. -H. Chen, X. -X. Yang, Z. -B. Wei, D. -H. Cao, M. Gu, and J. -T. Zhao, *Eur. J. Inorg. Chem.*, 2005, 4693.

23 H. B. Liang, Y. Tao, H. He, H. Wu, W. X. Chen, S. B. Wang, and Q. Su, *J. Solid State Chem.*, 2004, **177**, 901.

24 M. Kloss, B. Finke, L. Schwarz, and D. Haberland, *J. Lumin.*, 1997, **72–74**, 684.

25 Y-H. Lai, Y-C. Chang, T-F. Wong, W-J.Tai, W-J. Chang, and K-W. Lii, *Inorg. Chem.,* 2013, **52**, 13639.

26 M. Nazaraly, G. Wallez, C. Chaneac, E. Tronc, F. Ribot, M. Quarton, and J. P. Jolivet, *Angew. Chem., Int. Ed*. 2005, **44**, 5691.

27 M. A. Salvado, P. Pertierra, C. Trobajo, and J. P. Garcia, *J. Am. Chem. Soc.,* 2007, **129**, 10970.

28 M. Nazaraly, G. Wallez, C. Chaneac, E. Tronc, F. Ribot, M. Quarton, and J-P. Jolivet, *J. Phys. Chem. Solids.,* 2006, **67**, 1075.

29 M. Nazaraly, M. Quarton, G. Wallez, C. Chanea, F. Ribot, and J-P. Jolivet, *Solid State Sci.,* 2007, **9**, 672.

30 D. M. Bykov, E. Gobechiya, Y.K. Kabalov, A. I. Orlova, and S. V. Tomilin, *J. Solid State Chem.,* 2006, **179**, 3101.

31 N. Dacheux, N. Clavier, G. Wallez, and M. Quaton, *Solid State Sci.,* 2007, **9**, 619.

32 O.Terra, N. Dacheux, F. Audubert, and R. Podor, *J. Nucl. Mater.,* 2006, **352**, 224.

33 N. Clavier, N. Dacheux, and R. Podor, *Inorg. Chem.,* 2006, **45**, 220.

34 V. Brandel and N. Dacheux, *J. Solid State Chem.,* 2004, **177***,* 4755.

35 N. Clavier, G. Wallez, N. Dacheux, D. Bregiroux, M. Quarton, and P. Beaunier, *J. Solid State Chem.,* 2008, **181***,* 3352.

36 K. Popa, G. Wallez, D. Bregiroux, and P. Loiseau, *J. Solid State Chem.,* 2011, **184**, 2629.

37 G. Wallez, D. Bregiroux, K. Popa, P. E. Raison, C. Apostolidis, P. Lindqvist-Reis, R. J. M. Konings, and A. F. Popa, *Euro. J. Inorg. Chem.*, 2011, 110.

38 K. Popa, G. Wallez, P. E. Raison, D. Bregiroux, C. Apostolidis, P. Lindqvist-Reis, R. J. M. Konings, *Inorg. Chem.,* 2010, **49**, 6904.

39 G. Wallez, P. E. Raison, N. Dacheux, N. Clavier, D. Bykov, L. Delevoye, K. Popa, D. Bregiroux, A. N. Fitch, and R. J. M. Koning, *Inorg. Chem.,* 2012, **51**, 4314.

40 M-V. Le, D-S. Tsai, C-Y. Yang, Y-H. Chung, and H-Y Lee, *Electrochimica Acta.,* 2011, **56***,* 6654.

41 A. Borhan, B. Apetrăchioaei, and K. Popa, *Rev. Roum. Chim.,* 2010, **55**, 389.

42 K. Popa, D. Bregiroux, R. J. M. Konings, T. Goudera, A. F. Popad, T. Geislere, and P. E. Raison, *J. Solid State Chem.,* 2007, **180**, 2346.

43 Y. Xu, S. Feng, and W. Pang, *Mater. Lett.,* 1996, **28**, 499.

44 I.Szczygiel, *Thermochim. Acta.,* 2001, **370**, 125.

45 I. Szczygiel, *Thermochim. Acta.,* 2004, **417**, 75.

46 I Szczygieł, *Solid State Sci.,* 2006, **8**, 178.

47 I. Szczygiel, A. Matraszek, and T. Znamierowska, *J. Therm. Anal. Calor.,* 2008, **93**, 671.

48 I. Szczygieł, L. Macalik, T. Znamierowska, and J. Hanuza, *J. Alloys and Comp.,* 2004, **380**, 274.

49 I. V. Ogorodnyk, I. V. Zatovsky, V. N. Baumer, N. S. Slobodyanik, and O. V. Shishkin., *Acta Cryst.* C 2006, **62**, i100.

50 A. P. Hammersley, S. O. Svensson, M. Hanfland, A. N. Fitch, and D. Hausermann, Two-dimensional detector software: From real detector to idealized image or two-theta scan. *High Press. Res.,* 1996, **14**, 235.

51 J. Rodriguez-Carvajal, Fullprof 2000: A Program for Rietveld, Profile Matching and Integrated Intensity Refinements for X-ray and Neutron Data. Version 1.6, Laboratoire Leon Brillouin, Gif sur Yvette, France, **2000**.

52 V. Favre-Nicolin, and R. Cerný, *J. Appl. Cryst.,* 2002, **35**, 734.

53 D. D. Channei, B. Inceesungvorn, N. Wetchakun, S. Ukritnukun, and A. Nattestad, J. Chen, S. Phanichphant, *Nature Scientific Reports,* 2014, **4.** 5757.

54 P. Burroughs, A. Hamnett, A. F. Orchard, and G. Thornton, J. *Chem. Soc., Dalton Trans.,* **1976**, 1686.

55 N. Yu, V. V. Klepov, G. Modolo, D. Bosbach, E. V. Suleimanov, T. M. Gesing, L Robben, and E. V. Alekseev, *Inorg. Chem.,* 2014, **53**, 11231.

56 K. Asakura, Y. Satow, and H. Kuroda. *J. de Phys. Colloq.,* 1986, **47**, C8-185.

57 N. Galesic, B. Matkovic, M. Topic, E. Coffou, and M. Sljukic, *Croat. Chem. Acta.,* 1984, **57**, 597.

58 M. Doerffel and J. Liebert, *Z. Krist.,* 1990, **193**, 155.

59 S. K. Gupta, B. Rajeshwari, S. N. Achary, S. J. Patwe, A. K. Tyagi, V. Natarajan, and R. M. Kadam. *Eur. J. Inorg. Chem.* **2015**, 4429.

60 W. Geng, G. Zhu, Y. Shi, Y. Wang, *J. Lumin.,* 2014, **155**, 205.

61 Z.-w. Zhang, L. Liu, X. –f. Zhang, J. –p. Zhang, W.-g. Zhang, D. –j. Wang, *Spectrochim. Acta A* 2015, **137**, 1.

62 R. L. Frost and M. L. Weier, *J. Mol. Str.,* 2004, **697**, 207.

63 R. L. Frost, M. L. Weier, W. Martens, and J. Cejka, *Vibrational Spect.,* 2006, **41**, 205.

64 M. Harcharras, A. Ennaciri, A. Rulmont, and B. Gilbert, *Spectrochimica Acta A* 1997, **53**, 345.

Tables and Figure Captions

Table 1: Refined position coordinates of $K_2Ce(PO_4)_2$ and residuals of refinements.

Table 2: Typical inter-atomic distances in structure of $K_2Ce(PO_4)_2$.

Table 3: Typical bond angles in structure of $K_2Ce(PO_4)_2$.

Table 4: Observed Raman an IR modes of $K_2Ce(PO_4)_2$ and their assignments.

Fig.1: Powder XRD patters of different phases of $K_2Ce(PO_4)_2$ composition (λ = 1.5417Å). For comparison the data reported for $K_4Ce_2P_4O_{15}$ (a) (*ref 45*) and $K_2Ce(PO_4)$ H_2O (b) (*ref 43*) are shown as vertical lines.

Fig. 2: Typical thermogravimetric curves of $K_2Ce(PO_4)_2$ in heating cycle (a) and the DSC curves indicating the phase transition are shown in (b).

Fig. 3. Typical XRD patterns of $K_2Ce(PO_4)_2$ recorded at different temperatures (λ = 1.5417Å). The upward arrows indicate the evolving high temperature phase and asterisks indicate the peaks due to platinum sample holder. The XRD patterns at 550 and 600°C are representatives for the high temperature phase of $K_2Ce(PO_4)_2$.

Fig. 4: Rietveld refinement plot of the powder XRD pattern of $K_2Ce(PO_4)_2$ composition (λ = 0.8584 Å). Lower vertical ticks are the Bragg positions for monoclinic $CePO_4$.

Fig. 5: Crystal structure of $K_2Ce(PO_4)_2$ in 100 projection. The CeO_8 (pink) and PO_4 tetrahedra (green and grey) are shown. Isolate spheres are K1 (blue) and K2 (red). Small (cyan) spheres indicate polyhedral corner oxygen atoms.

Fig. 6: Typical connections of distorted cubic MO_8 polyhedra and tetrahedral PO_4 in different $A_2M(PO_4)_2$ structures. $(NH_4)_2Ce(PO_4)_2H_2O$ (a.) *ref 27,49*), (b) and (c) for $Na_2Th(PO_4)_2$(*ref 57*) and (d) $K_2Ce(PO_4)_2$ of present study. Pink and blue spheres are M^{4+} cations. , Yellow and cyan spheres are P^{5+} and O^{2-} ions.

Fig. 7: XPS spectra of $K_2Ce(PO_4)_2$.

Fig. 8: XANES spectra of $K_2Ce(PO_4)_2$ and CeO_2 around the L-II edge.

Fig. 9: Typical Raman spectrum of $K_2Ce(PO_4)_2$.

Fig. 10: Typical IR spectrum of $K_2Ce(PO_4)_2$.

Table 1: Refined position coordinates of $K_2Ce(PO_4)_2$ and residuals of refinements.

Atoms	*wyc.*	x	y	z	Uiso(Å)^2
Ce1	*4e*	0.2785(2)	0.1402(2)	0.0237(4)	0.0147(6)
K1	*4e*	0.4522(8)	0.1275(8)	0.6028(10)	0.016(2)
K2	*4e*	0.0456(8)	0.1139(7)	0.3795(10)	0.031(3)
P1	*4e*	0.8437(5)	0.1458(4)	0.7885(5)	0.018(3)
P2	*4e*	0.3641(4)	0.8740(4)	0.8304(6)	0.014(3)
O11	*4e*	0.7531(14)	0.2693(8)	0.772(2)	0.019(3)
O12	*4e*	1.0053(9)	0.1413(17)	0.9517(15)	0.019(3)
O13	*4e*	0.7643(18)	0.0215(10)	0.805(3)	0.019(3)
O14	*4e*	0.8714(14)	0.1506(16)	0.6005(10)	0.019(3)
O21	*4e*	0.4823(12)	0.8415(15)	1.0306(10)	0.018(3)
O22	*4e*	0.2642(14)	0.7540(8)	0.764(2)	0.018(3)
O23	*4e*	0.2541(15)	0.9827(11)	0.832(3)	0.018(3)
O24	*4e*	0.4637(15)	0.9063(13)	0.7094(17)	0.018(3)

a = 9.1060(4), b = 10.8160(4), c = 7.6163(4) Å, β = 111.155(2)°

V = 700.50(6) Å^3, Z = 4, $\rho_{x\text{-}ray}$ = 3.87 g/cc

R_p = 5.45 %, R_{wp} = 6.44 %, and χ^2 = 2.97

Table 2: Typical inter-atomic distances in structure of $K_2Ce(PO_4)_2$.

Bonds	Dist. (Å)	Bonds	Dist. (Å)	Bonds	Dist. (Å)	Bonds	Dist. (Å)	Bonds	Dist. (Å)
Ce1-O12	2.346(9)	P1-O11	1.551(11)	P2-O21	1.558(9)	K1-O11	2.996(13)	K2-O11	2.637(17)
Ce1-O23	2.204(16)	P1-O12	1.548(11)	P2-O22	1.561(11)	K1-O11	2.756(13)	K2-O13	2.980(19)
Ce1-O22	2.422(13)	P1-O13	1.553(14)	P2-O23	1.547(14)	K1-O12	2.867(19)	K2-O14	2.728(15)
Ce1-O13	2.299(16)	P1-O14	1.544(10)	P2-O24	1.549(14)	K1-O13	2.934(16)	K2-O14	2.949(19)
Ce1-O21	2.368(11)					K1-O21	2.661(11)	K2-O21	2.592(17)
Ce1-O24	2.541(13)					K1-O22	2.869(17)	K2-O22	3.048(14)
Ce1-O11	2.217(14)					K1-O24	2.517(16)	K2-O22	2.995(13)
Ce1-O14	2.412(17)					K1-O24	2.776(17)	K2-O23	2.822(14)
						K1-O23	3.32(2)	K2-O12	3.163(14)
						K1-O13	3.425(19)	K2-O23	3.577(20)

Table 3: Typical bond angles in structure of $K_2Ce(PO_4)_2$.

	Angle. (°)		Angle. (°)		Angle. (°)
O12-Ce1-O23	90.2(6)	O11-P1-O12	114.6(9)	O21-P2-O22	104.2(8)
O12-Ce1-O22	88.6(5)	O11-P1-O13	120.2(8)	O21-P2-O23	112.6(10)
O12-Ce1-O13	75.8(6)	O11-P1-O14	99.0(8)	O21-P2-O24	106.8(7)
O12-Ce1-O21	157.4(4)	O12-P1-O13	104.1(10)	O22-P2-O23	109.3(8)
O12-Ce1-O24	141.6(4)	O12-P1-O14	108.8(6)	O22-P2-O24	113.1(8)
O11-Ce1-O12	76.6(5)	O13-P1-O14	110.0(10)	O23-P2-O24	110.7(9)
O12-Ce1-O14	107.6(6)				
O22-Ce1-O23	81.2(5)		Ce1-O12-P1	144.0(6)	
O13-Ce1-O23	78.0(6)		Ce1-O13-P1	152.1(13)	
O21-Ce1-O23	80.1(5)		Ce1-O14-P1	95.5(7)	
O23-Ce1-O24	102.8(6)		Ce1-O21-P2	99.4(5)	
O11-Ce1-O23	153.1(5)		Ce1-O22-P2	126.9(8)	
O14-Ce1-O23	146.0(5)		Ce1-O23-P2	133.0(11)	
O13-Ce1-O22	153.7(6)		Ce1-O24-P2	92.8(6)	
O21-Ce1-O22	69.9(4)				
O22-Ce1-O24	128.8(5)				
O11-Ce1-O22	121.2(4)				
O14-Ce1-O22	70.8(3)				
O13-Ce1-O21	121.2(6)				
O13-Ce1-O24	72.0(6)				
O11-Ce1-O13	76.1(5)				
O13-Ce1-O14	133.8(5)				
O21-Ce1-O24	61.0(4)				
O11-Ce1-O21	119.9(4)				
O14-Ce1-O21	72.6(5)				
O11-Ce1-O24	75.8(5)				
O14-Ce1-O24	81.4(4)				
O11-Ce1-O14	60.9(4)				

Table-4. Observed Raman an IR modes of $K_2Ce(PO_4)_2$ and their assignments.

Raman (ω cm^{-1})	IR (ω cm^{-1})		Assignments
116			
124			
156			
163			
178			
202			Lattice modes
214			
226			
236			
248			
271			
312			
396	392		
402		ν2	δs (Symmetric bending)
450			
461	482		
542	542		
549	555		
564	577	ν2	δas (asymmetric bending)
581			
590	594		
608	625		
628			
943	941		
960	957		
983	986	ν1	ν_s (asymmetric bending)
997			
1001			
1022	1013		
1038	1067	ν3	ν_{as} (asymmetric bending)
	1092		
1129	1128		

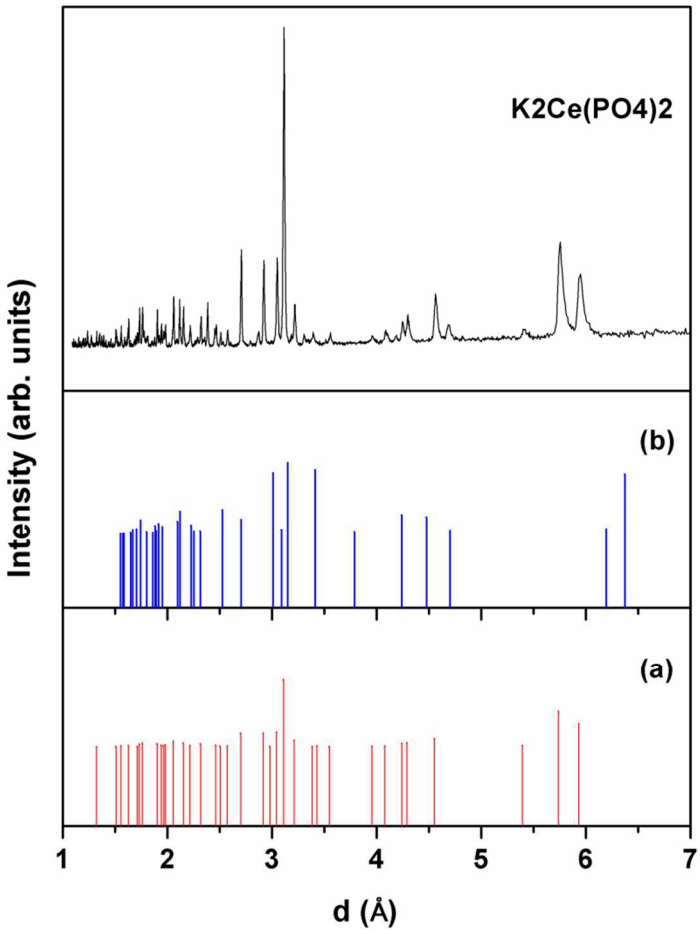

Fig.1: Powder XRD patters of different phases of $K_2Ce(PO_4)_2$ composition (λ = 1.5417Å). For comparison the data reported for $K_4Ce_2P_4O_{15}$ (a) (*ref 45*) and $K_2Ce(PO_4)\ H_2O$ (b) (*ref 43*) are shown as vertical lines.

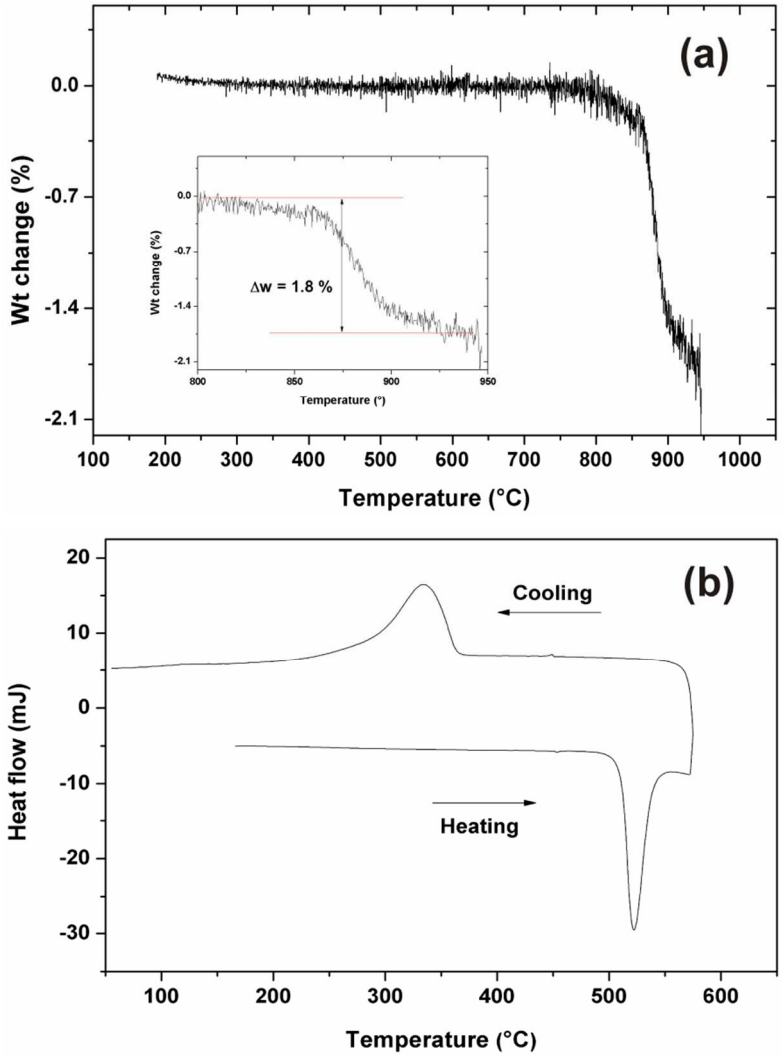

Fig. 2: Typical thermogravimetric curves of $K_2Ce(PO_4)_2$ in heating cycle (a) and the DSC curves indicating the phase transition are shown in (b).

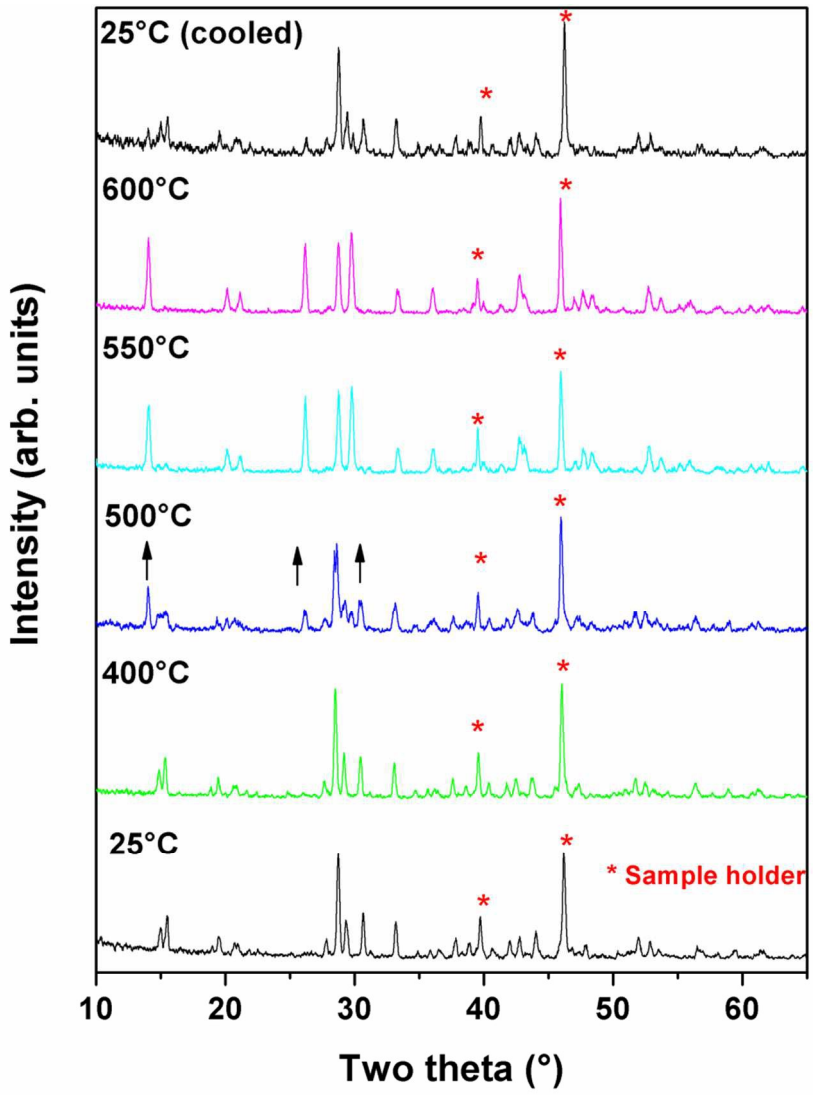

Fig. 3. Typical XRD patterns of $K_2Ce(PO_4)_2$ recorded at different temperatures ((λ = 1.5417Å). The upward arrows indicate the evolving high temperature phase and asterisks indicate the peaks due to platinum sample holder. The XRD patterns at 550 and 600°C are representatives for the high temperature phase of $K_2Ce(PO_4)_2$.

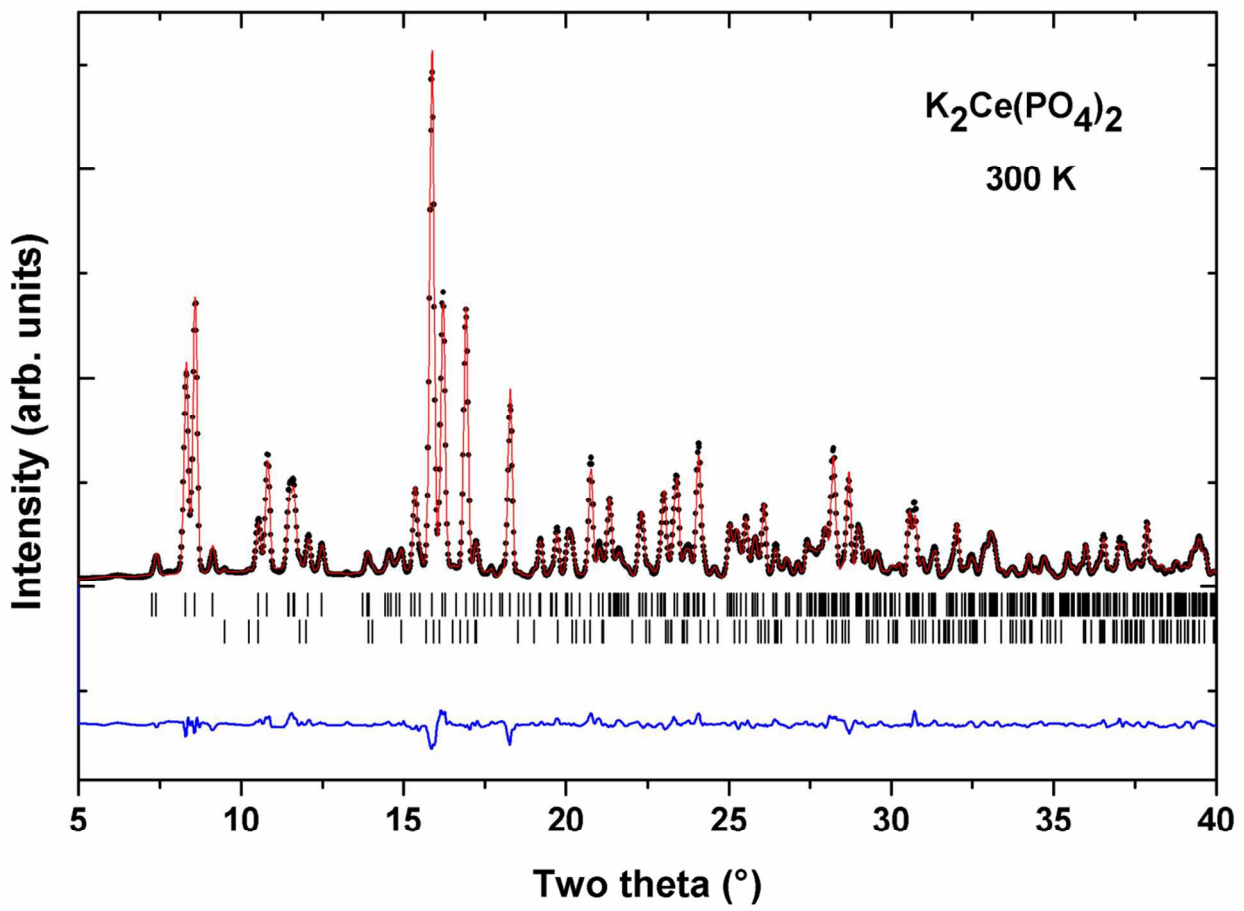

Fig. 4: Rietveld refinement plot of the powder XRD pattern of $K_2Ce(PO_4)_2$ composition (λ = 0.8584 Å). Lower vertical ticks are the Bragg positions for monoclinic $CePO_4$.

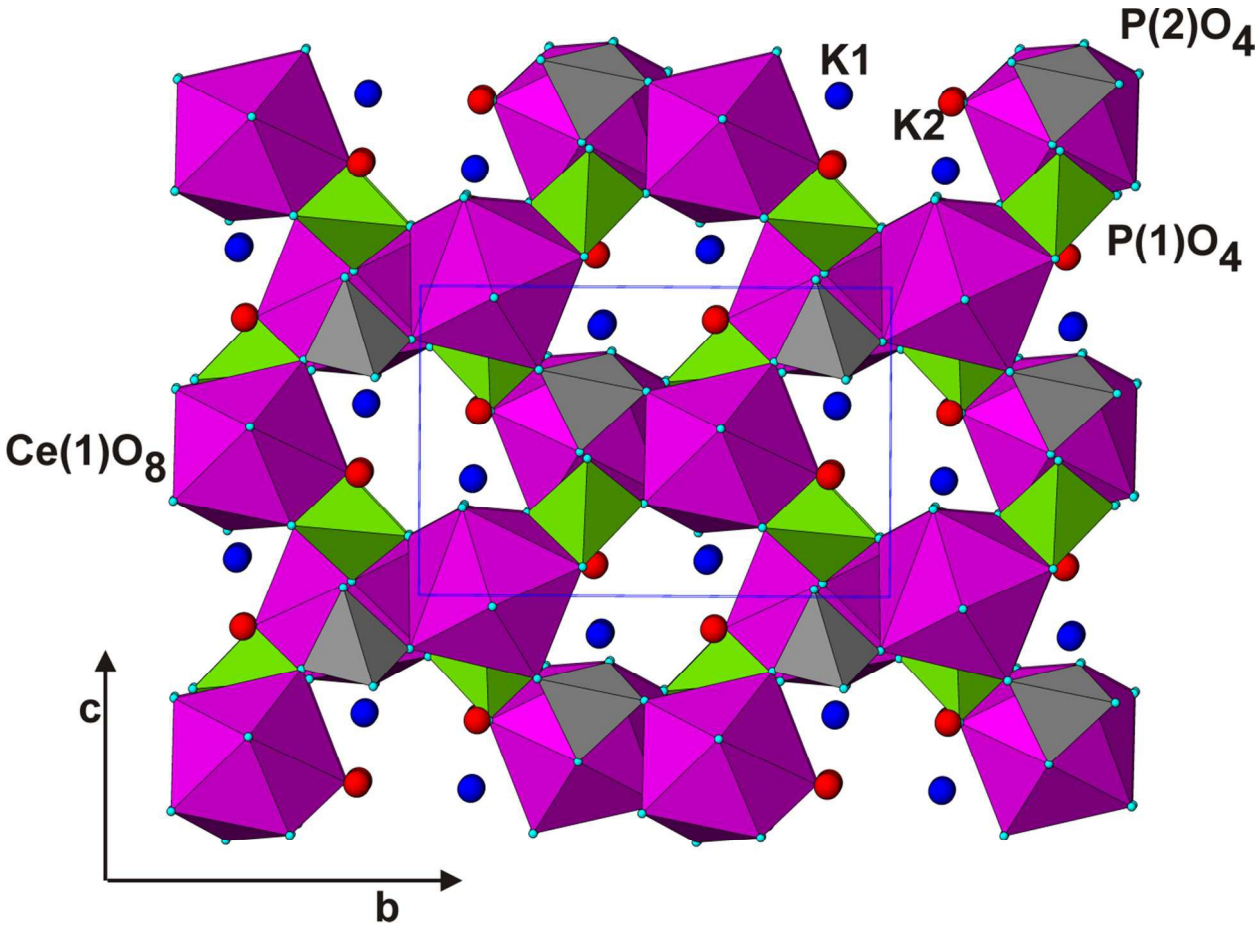

Fig. 5: Crystal structure of $K_2Ce(PO_4)_2$ in 100 projection. The CeO_8 (pink) and PO_4 tetrahedra (green and grey) are shown. Isolate spheres are K1 (blue) and K2 (red). Small (cyan) spheres indicate polyhedral corner oxygen atoms.

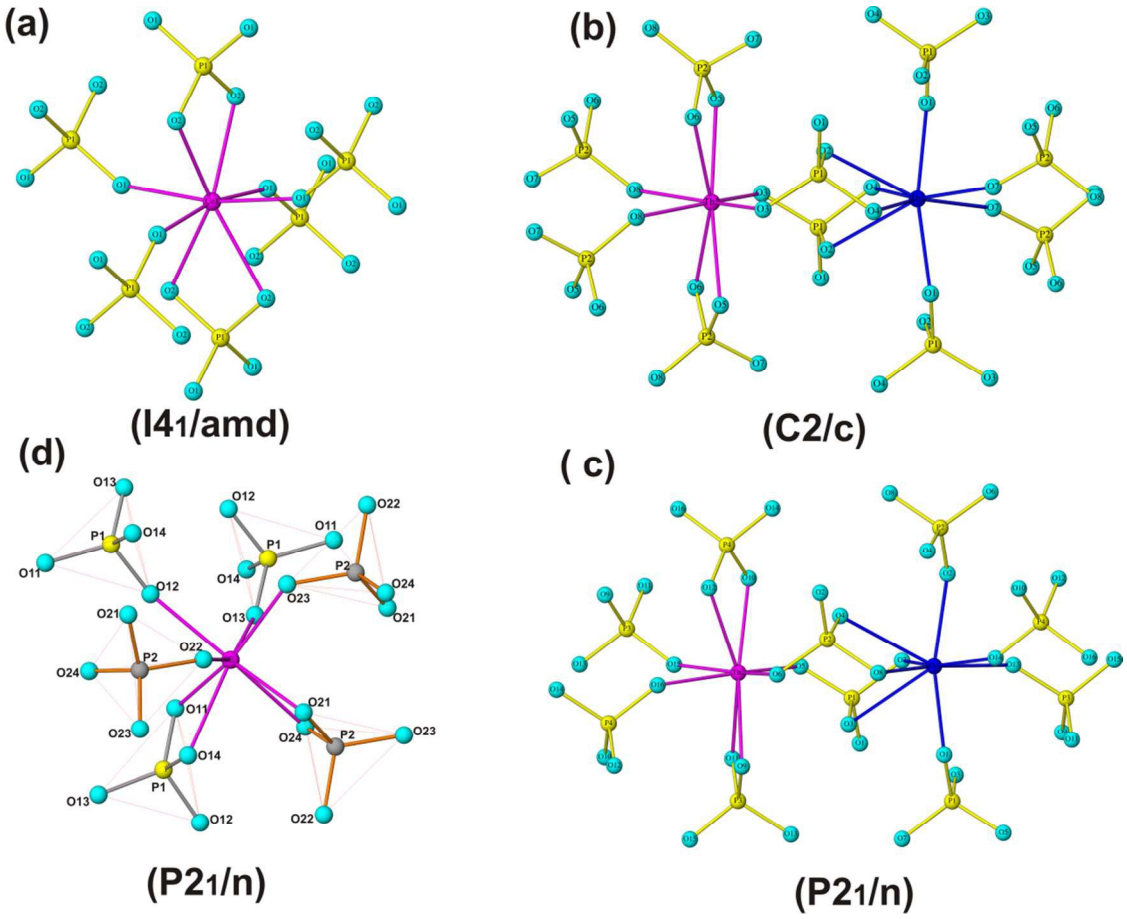

Fig. 6: Typical connections of distorted cubic MO_8 polyhedra and tetrahedral PO_4 in different $A_2M(PO_4)_2$ structures. $(NH_4)_2Ce(PO_4)_2H_2O$ (a.) *ref 27,49*), (b) and (c) for $Na_2Th(PO_4)_2$(*ref 57*) and (d) $K_2Ce(PO_4)_2$ of present study. Pink and blue spheres are M^{4+} cations. , Yellow and cyan spheres are P^{5+} and O^{2-} ions.

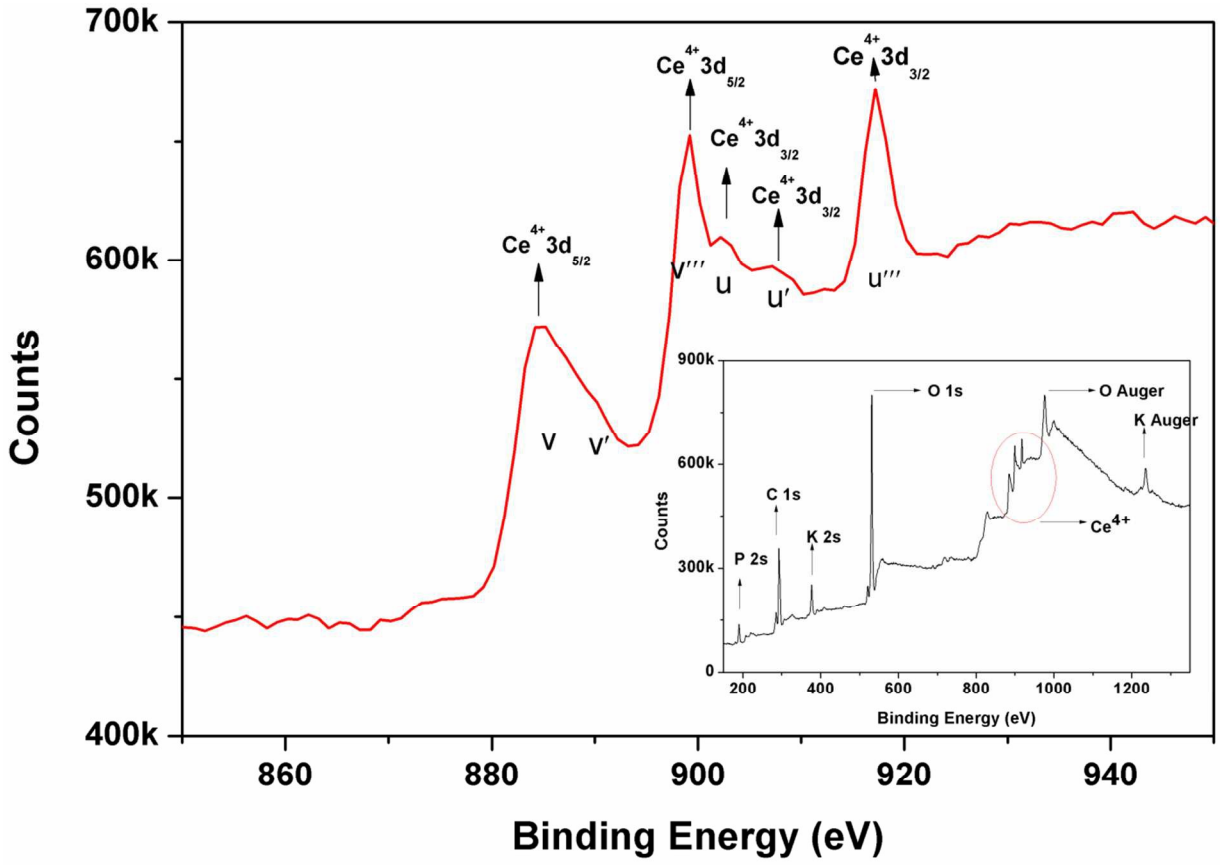

Fig. 7: XPS spectra of $K_2Ce(PO_4)_2$.

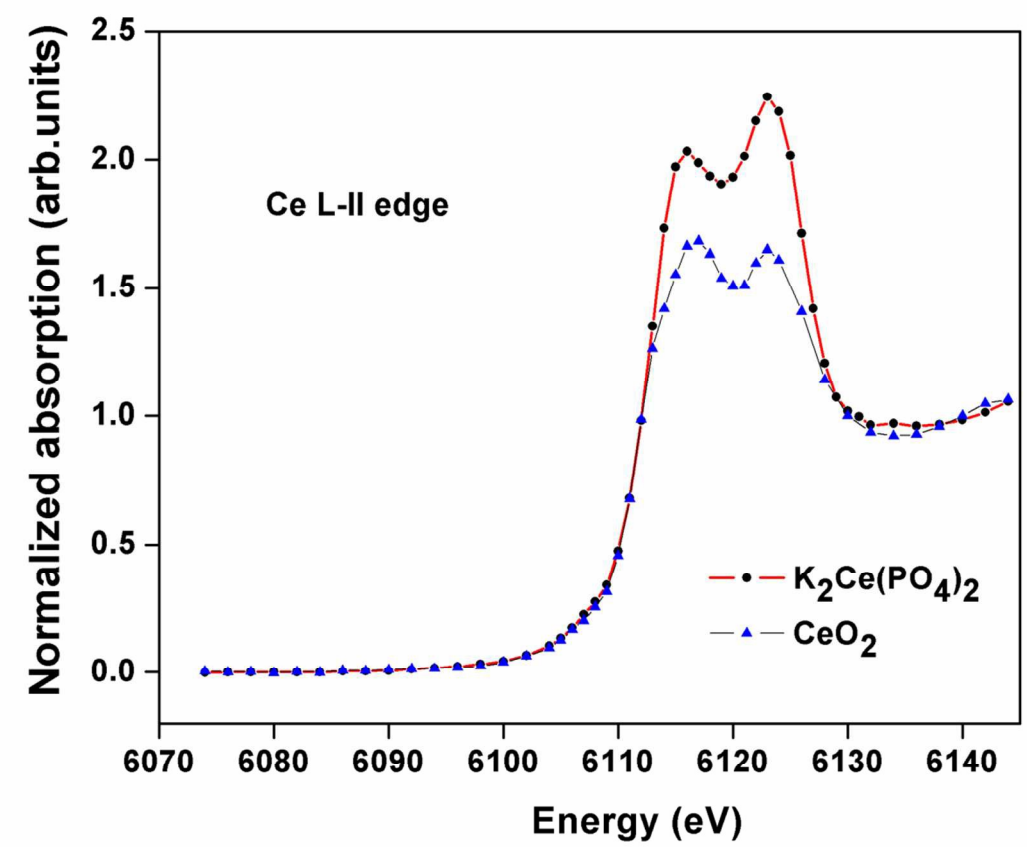

Fig. 8: XANES spectra of $K_2Ce(PO_4)_2$ and CeO_2 around the L-II edge.

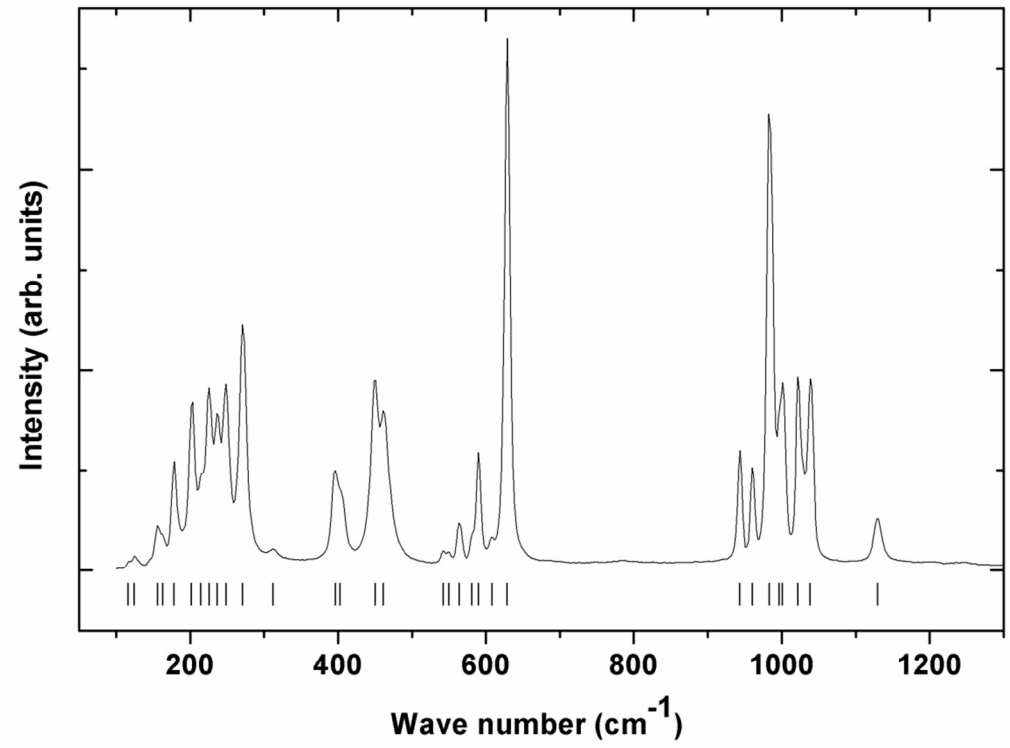

Fig. 9: Typical Raman spectrum of $K_2Ce(PO_4)_2$.

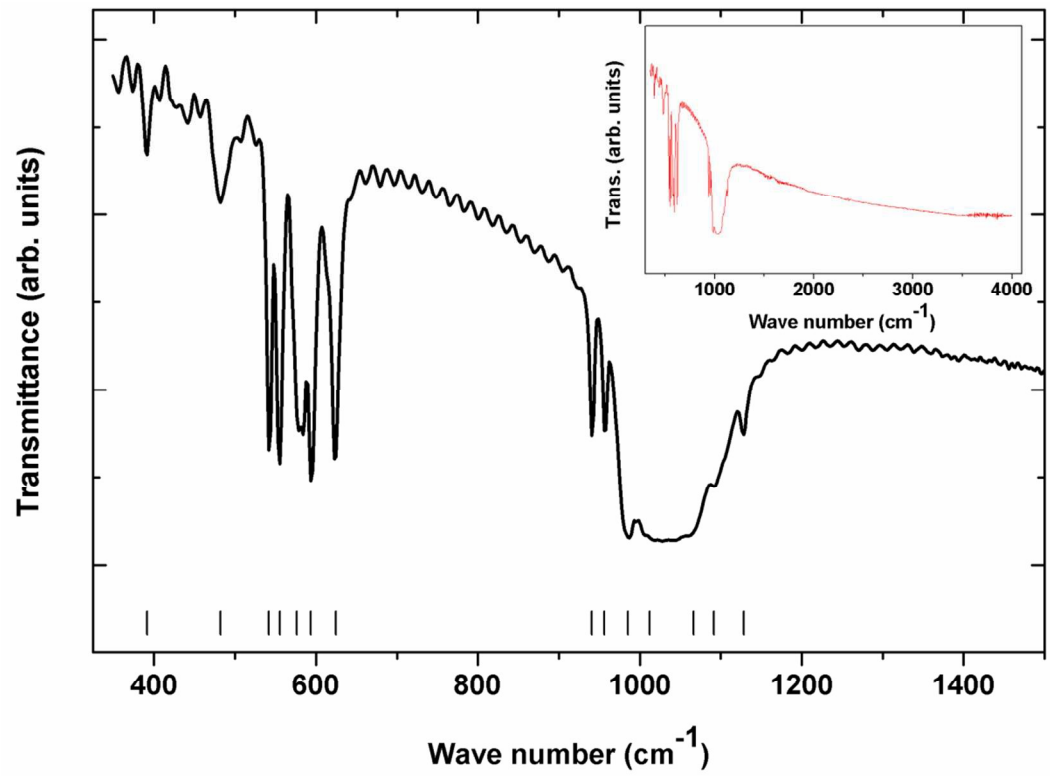

Fig. 10: Typical IR spectrum of $K_2Ce(PO_4)_2$.

Graphical Abstract

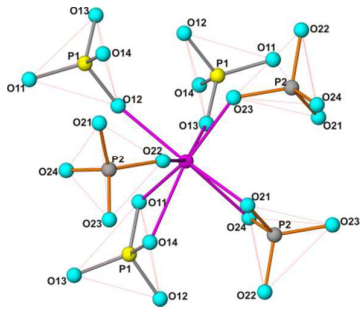

Synthesis and crystal structure of $K_2Ce(PO_4)_2$, a new complex phosphate with Ce^{4+}.